This Original Research Article has been accepted for publication in Vol. 36, No. 10, of the Journal of Mechanical Science and Technology 10 (2022)
Journal website: https://www.springer.com/journal/12206

Design and experimental testing of a tactile sensor for self-compensation of contact error in soft tissue stiffness measurement

Frank Efe Erukainure[1,2], Victor Parque[1,3], Mohsen A. Hassan[4] and Ahmed M. R. FathEl-Bab[1]

[1]Department of Mechatronics and Robotics Engineering, Egypt-Japan University of Science and Technology, New Borg El-Arab City, 21934, Alexandria, Egypt, [2]Department of Mechanical and Mechatronics Engineering, Federal University Otuoke, P.M.B. 126, Yenagoa, Bayelsa State, Nigeria, [3]Department of Modern Mechanical Engineering, Waseda University, Tokyo 169-8555, Japan, [4]Department of Materials Science and Engineering, Egypt-Japan University of Science and Technology, New Borg El-Arab City, 21934, Alexandria, Egypt

(Received Feb 13, 2022; Revised Jun 15, 2022; Accepted Jun 26, 2022)

Keywords: ANSYS Mechanical APDL; Fruit quality and sorting; Kiwifruit elastic modulus; Kiwifruit tissue stiffness; Surface roughness; Tactile sensing

Correspondence to: Frank Efe Erukainure / frank.erukainure@ejust.edu.eg

Abstract The measurement of viscoelastic properties of soft tissues has become a research interest with applications in the stiffness estimation of soft tissues, sorting and quality control of postharvest fruit, and fruit ripeness estimation. This paper presents a tactile sensor configuration to estimate the stiffness properties of soft tissues, using fruit as case study. Previous stiffness-measuring tactile sensor models suffer from unstable and infinite sensor outputs due to irregularities and inclination angles of soft tissue surfaces. The proposed configuration introduces two low stiffness springs at the extreme ends of the sensor with one high stiffness spring in-between. This study also presents a closed form mathematical model that considers the maximum inclination angle of the tissue's (fruit) surface, and a finite element analysis to verify the mathematical model, which yielded stable sensor outputs. A prototype of the proposed configuration was fabricated and tested on kiwifruit samples. The experimental tests revealed that the sensor's output remained stable, finite, and independent on both the inclination angle of the fruit surface and applied displacement of the sensor. The sensor distinguished between kiwifruit at various stiffness and ripeness levels with an output error ranging between 0.18% and 3.50%, and a maximum accuracy of 99.81%, which is reasonable and competitive compared to previous design concepts.

1. Introduction

Over the past four decades, it has been reported in several studies and field observations that 40-50% of crops produced in developing countries are lost before they are consumed, mainly due to high rates of bruising, water loss, and subsequent decay during postharvest handling. The main causes of postharvest losses include rough handling, lack of good temperature management system, poor packaging material, and lack of public awareness about the need to maintain quality [1]. On the other hand, fruits are harvested when mature and it is often challenging to avoid postharvest losses. When the harvested fruits are stored under far from the ideal conditions, they ripen quickly and lose their hardness (stiffness) over a short period. Moreover, the change in colour does not necessarily imply the ripeness of most fruit; in most cases, ripeness is determined by touching the fruit with the hands while applying little force with the fingers (pressing the fruit). However, the touch-based method to estimate ripeness often leads to further deterioration of the fruit's quality (such as taste and appearance), hence changing its mechanical properties (such as hardness or stiffness).

Kiwifruit (*Actinidia deliciosa*), which is the case study of this paper, is a soft, tender, and nutritious fruit; it suffers from mechanical compression damage quickly in various forms during picking, packaging, transporting, and marketing [2]. Due to the appearance of the kiwifruit, it is difficult to determine its quality and mechanical properties without touching the fruit's surface and applying some form of pressure on the surface. Hence, being of relevant concern to farmers and marketers, the quality of the fruit is negatively affected, as aforementioned. Effective ripeness detection devices, such as tactile sensors, are potential mechanisms to tackle the aforementioned challenges.

Several studies have been carried out on fruit sorting and ripeness detection based on: acoustic vibration technology as reported in [3], gas sensors and electronic nose [4], as well as computer vision and image processing techniques [5], [6], [7], [8], [9], [10]. Optical techniques which focus on interactions between light and soft tissue stiffness have equally been developed to estimate the internal quality of fruit as reported by [11], [12], [13], [14]. In [11], two major methods of optical techniques were reported: "image analysis with laser light, and laser photon counting spectroscopy". The near-infrared and laser excitation methods were reported in [12]. However, the research on fruit sortation based on the relation between the stiffness constant K and elasticity has received little attention. The stiffness constant is relevant in measuring the mechanical properties of fruit tissues [15].

The use of tactile sensors for soft tissue stiffness measurement is advantageous when compared with other techniques because it is based on direct contact with the object's tissue,

whereas other techniques previously mentioned above are based on indirect or non- contact with the object. Hence, the real sense of touch is compromised, and this could lead to misclassifications in ripeness or stiffness measurement as experienced by [16] and [17] when the authors tried to sort carrot's quality using image processing technique.

The mechanical properties and compression damage simulation by finite element modelling for kiwifruit was reported by [18], where it was found that the average elastic modulus of kiwifruit's flesh on radial loading is 1.71 MPa. Similarly, the mechanical properties of banana was studied by [19] under quasi-static loading; the mechanical properties of potato under creep loading was studied by [20] using experiments and finite element analysis. The authors postulated that it is possible to improve the storage life and reduce wastage of food crops when the mechanical properties of their tissues are known. However, the process of carrying out the compression (or loading) tests and calculating the mechanical properties is implicitly destructive in its nature and time consuming. The use of tactile sensors are prospective mechanisms to enable non-destructive testing and ensure just-in-time measurement of the mechanical properties of fruit tissues.

Tactile sensors for fruit stiffness measurement have equally been developed in recent studies by [21], [22], [23], albeit studies are limited in this application. A tactile sensing alternative for robotic force sensing was proposed by [24]. The device uses a force sensor and an end-effector to sense the force of a tissue in contact. Similarly, [25] proposed a piezoelectric tactile sensor for measuring soft tissue damping coefficient. However, the sensors proposed by [24] and [25] have focused more on material handling and force sensing without considering the contact error and stiffness of soft tissues such as fruit tissues. Thus, more work is required in this direction.

In [23], [26], [27], a two-tip tactile sensor configuration was proposed for stiffness measurement of soft tissues; however, the disadvantage of the two-tip configuration is that the sensor's output is only stable in FEM analysis. When used experimentally to measure the stiffness of soft tissues (such as fruit tissue), the output becomes unstable and prone to errors due to the surface irregularity of soft tissues and the angle of inclination of their surfaces. In [28], the output of the proposed sensor configuration was stable only when there was no inclination angle on the surface of the tissue being measured. At an inclination angle of 6^0, the output rendered unstable and with infinite values; a number of fluctuations in the output signals were also observed. An error rate of 14% was recorded in the sensor's output with respect to analytical observations. The 14% error rate is large enough to offer inaccurate results for stiffness detection, which could imply the unsafe and risky decision making for biomedical applications, as well as the unviable assessments for fruit classification and marketing.

1.1 Contributions

This paper aims to present the design, modeling, and experimental testing of a tactile sensor configuration that addresses the shortfalls mentioned above. The proposed sensor will be helpful in measuring the stiffness properties (such as the stiffness constant, elastic modulus, and eventually, the ripeness) of fruit in a non-destructive manner. Since the tissue of most fruit is soft in nature, the fruit can be referred to as a *soft tissue*; and the kiwifruit tissue is a case study in this paper.

Thus, the main contributions of this paper are to:

1) Propose a design configuration for a tactile sensor that allows the self-compensation of contact error caused by inclination angles and surface irregularities of soft tissues. The sensor proposed in this paper is aimed at solving the challenges experienced by [23], [26], and [27]. Its basic architecture combines two low stiffness springs at the extreme ends of the sensor with one high stiffness spring in-between.
2) Present the closed-form mathematical relationships to determine the sensor design parameters to enable stable sensor outputs that directly relate to changes in stiffness of soft tissues.
3) Study the range of elastic modulus of distinct kiwifruit specimens and the inclination angles across the surface of the kiwifruit tissue. These studies are relevant on their own, as they help in deciding the sensor's configuration to avoid the errors of unstable, infinite, and zero output encountered by previous researchers such as [28].
4) Evaluate the sensor's performance by dynamic simulations based on Finite Element Method (FEM) of a 3D axisymmetric model of the fruit tissue.
5) Evaluate the performance of the proposed sensor configuration experimentally. The results from experiments showed that the sensor's output is stable over independent trials and agrees with the observations derived from the dynamic simulations. The sensor's output was also independent of the inclination angle of the kiwifruit tissue surface. Small error rates of 0.18% to 3.50% between the analytical and experimental outputs were observed, with a maximum accuracy of 99.81%. The results are competitive compared to the current state-of-the-art design concepts of tactile sensors used in stiffness measurements.

2. Proposed sensor configuration

This section describes the basic idea and key mathematical formulations behind the proposed sensor configuration.

2.1 Basic concept

The proposed configuration for the tactile sensor is made while bearing in mind that the surface of the fruit tissue is irregular. The concept is inspired by a cantilever beam model whose architecture comprises three linear springs, as shown by Fig. 1(a), in which:

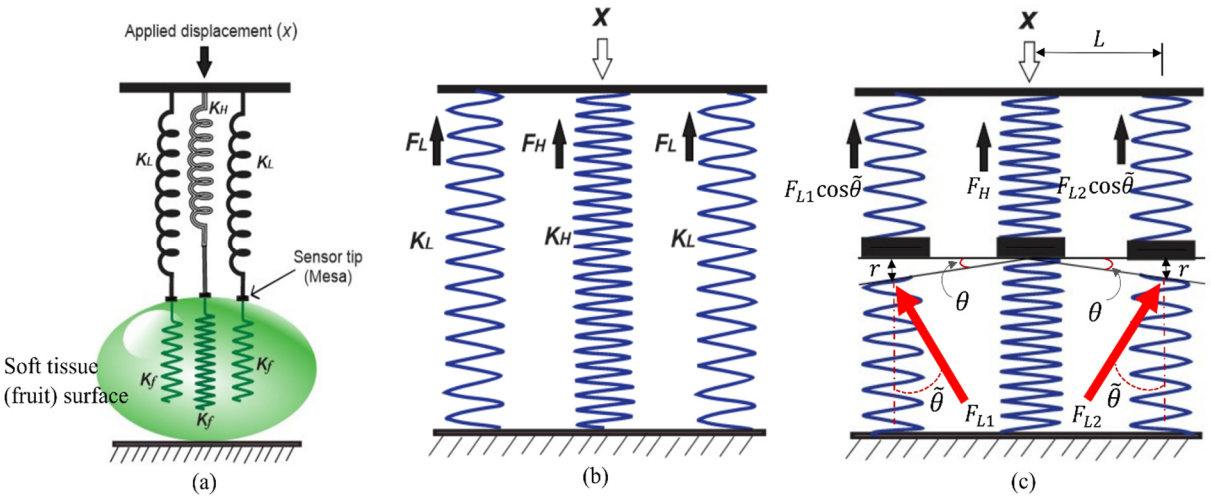

Fig. 1(a) The sensor model; (b) Equivalent sensor model; (c) Equivalent sensor model with an inclination angle.

- The stiffness of the central spring is K_h, and is labeled as a *high stiffness spring* due to its relatively high stiffness value compared to other springs in the system.
- Two springs, each of which has the stiffness K_l, are located at the extreme sides of the sensor; and both are labeled as *low stiffness springs* due to $K_l < K_h$.
- Each of the three springs has a tip for direct contact with the tissue being measured, and the distance between the three tips must be as small as possible to minimize the contact error.
- A relevant configuration of the above enables the tackling of the inclination angle of the fruit's tissue surface, which is a unique point compared to previous studies.

In the next section, the basic mathematical principles behind the configuration of the sensor is presented.

2.2 Mathematical Modeling

Fig. 1(a) shows the overall configuration of the sensor, which consists of three linear springs (two springs with stiffness K_l and one spring with stiffness K_h) and three tips attached to the end of each spring. Also, in Fig. 1(a), the stiffness of the measured specimen is modeled as an elastic spring with stiffness K_f. As such, when the sensor is displaced by a distance x in the vertical direction, concomitant forces are generated along each spring. The equivalent model which corresponds to the sensor-specimen configuration can be represented by a three-spring system as shown by Fig. 1(b). Here, for a displacement x in the vertical direction, the concomitant forces generated in both the *low* and the *high* stiffness springs will be denoted by F_L and F_H, respectively. Due to the nature of the three-springs configuration and the contact with the measured specimen, the spring stiffness K_l and K_h in Fig. 1(a) are in series with the fruit stiffness K_f; therefore, the equivalent stiffness K_H and K_L in Fig. 1(b) can be expressed as follows:

$$K_H = \frac{K_h K_f}{K_h + K_f} \tag{1}$$

$$K_L = \frac{K_l K_f}{K_l + K_f} \tag{2}$$

where:

- K_H denotes the equivalent stiffness of the central spring in the equivalent sensor model,
- K_L denotes the equivalent stiffness of the springs located at the extremes of the equivalent sensor model.

The above-mentioned formulations assume that no inclination angle occurs during the contact between the sensor tips and the measured specimen. Due to this fact, the central spring of the equivalent model at Fig. 1(b) will generate a higher force F_H while the outer springs of the equivalent model will each generate the same magnitude of lower force F_L, implying that the condition $F_H > F_L$ fulfills. Thus, by using the equivalent forces F_H and F_L, the stiffness K_f of the measured specimen as well as the sensor output can be calculated from the following relations:

$$S = \frac{F_H}{2F_L} = \frac{K_H}{2K_L} = \frac{K_h(K_l + K_f)}{2K_l(K_h + K_f)} \tag{3}$$

where S denotes the sensor output as a dimensionless parameter. On the other hand, when an inclination angle θ between the sensor tips and the surface of the measured specimen occurs, the configuration of the equivalent model will differ since the generated forces along the springs will not be co-linear. As such, Fig. 1(c) shows the configuration of the equivalent model when the inclination angle θ is considered, wherein:

- The central spring of the sensor has contact to the central spring of the measured specimen at 90^0.
- θ denotes the inclination angle of the springs located at the

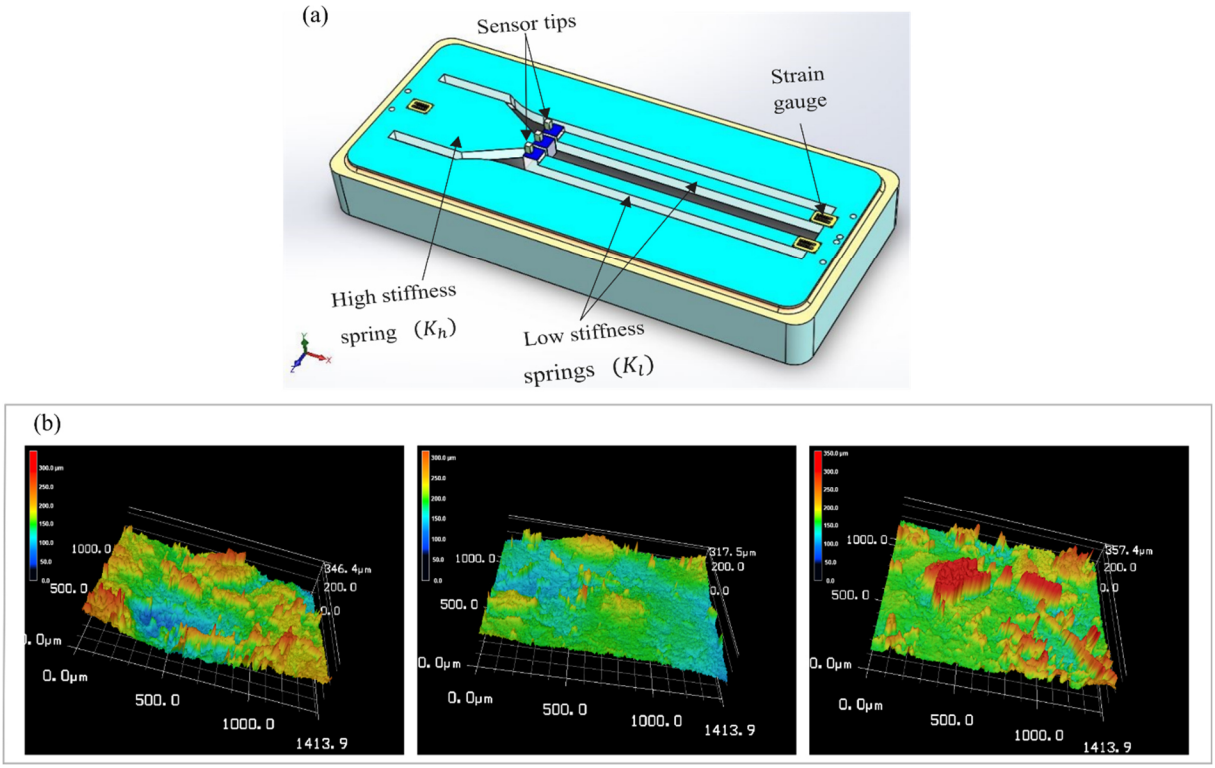

Fig. 2. (a) Proposed tactile sensor prototype. (b) 3D surface profiles of kiwifruit.

extremes of the measured specimens, and $\tilde{\theta}$ denotes the vertical component due to the inclination.

- L denotes the separating distance between the spring elements.
- Two important reaction forces will be generated at the surface of the measured specimen: (1) F_{L1}, which is the force generated at the left side of the central spring, and (2) F_{L2}, which is the force generated at the right side of the central spring.
- Two reaction force components are generated due to the inclination: (1) $F_{L1}\cos\tilde{\theta}$ being the force generated at the left side of the sensor configuration, and (2) $F_{L2}\cos\tilde{\theta}$ being the force generated at the right side of the sensor configuration.

Therefore, when the inclination angle $\theta > 0$ occurs in Fig. 1(c), the forces F_{L1} and F_{L2} will either be the same, if the inclination angles to the left and right side are equal, or will differ, if otherwise. Likewise, the force F_H at the *higher stiffness spring* will be different from F_{L1} and F_{L2}. For simplicity and without loss of generality, this study considers the case when the inclination angles at the two extremes, that is the *low stiffness springs*, are equal, while the inclination angle at the central spring, that is the *higher stiffness spring*, maintains a perpendicular contact with the surface of the specimen. Thus, the sensor output can be expressed as a ratio of the high and low stiffness spring forces, as follows.

$$S = \frac{F_H}{F_{L1}\cos\tilde{\theta} + F_{L2}\cos\tilde{\theta}} \tag{4}$$

$$\left.\begin{aligned} F_{L1} = F_{L2} = F_L = K_L(x - L\tan\theta) \\ F_H = xK_H \end{aligned}\right\} \tag{5}$$

where L denotes the distance between the sensor tips, and x denotes the displacement in the vertical direction. In the above formulations, it is possible to neglect the term $L\tan\theta$ for small values of length L and inclination angle θ, thus the sensor output becomes:

$$S = \frac{F_H}{2F_L\cos\tilde{\theta}} = \frac{K_H}{2K_L\cos\tilde{\theta}} = \frac{K_h(K_l+K_f)}{2K_l(K_h+K_f)\cos\tilde{\theta}} \tag{6}$$

It should be noted, however, that $\cos\tilde{\theta}$ approximately equals 1 since $\tilde{\theta}$ is within the limit of the inclination angle (i.e., $0 \leq \tilde{\theta} < 6^0$). Thus, Eq. (6) becomes

$$S = \frac{K_h(K_l+K_f)}{2K_l(K_h+K_f)} \tag{7}$$

Accordingly, the reader may note that Eq. (7) renders an equivalent formulation to Eq. (3), in which the sensor output is independent of the angle θ. Rewriting Eq. (7), the stiffness of the fruit can be calculated as follows:

$$K_f = \frac{K_hK_l(1-2S)}{2SK_l - K_h} \tag{8}$$

Thus, the above-mentioned formulation at Eq. (8) represents a closed form expression to estimate the stiffness of the fruit as a function of not only the sensor output S, but also the *high stiffness spring* K_h and the *low stiffness springs* K_l.

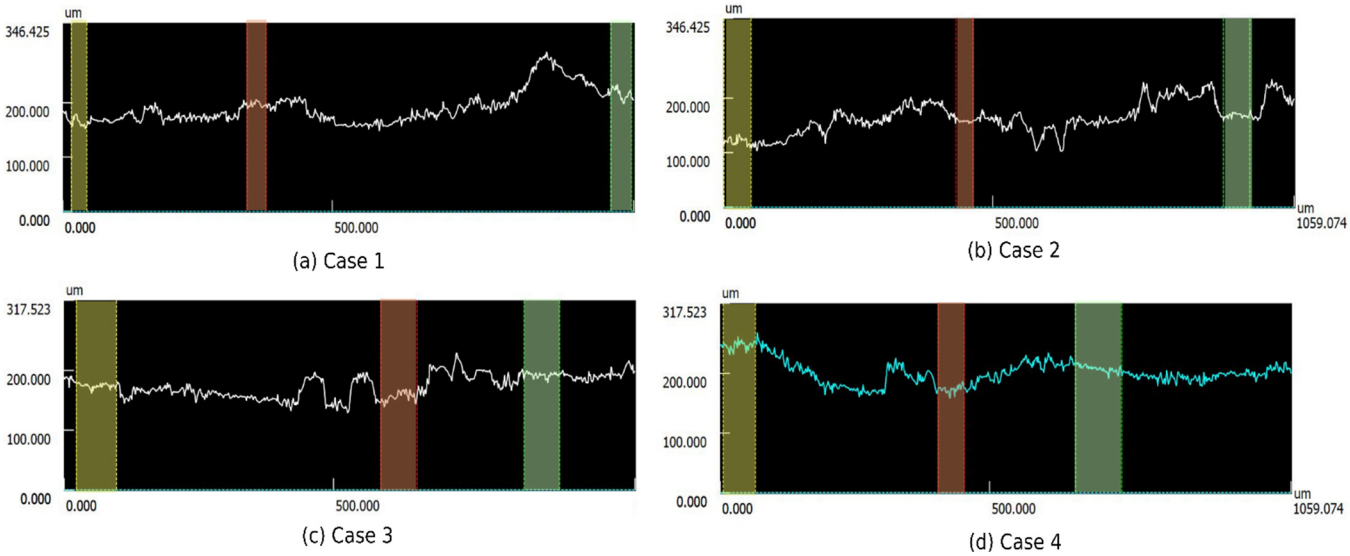

Fig.3. Peaks, valleys, and profiles of sample kiwifruit.

3. Design considerations

This section describes the key motivations behind the design and experimental realization of the proposed sensor configuration. Although the sensor is expected to estimate the stiffness of soft bodies (tissues) in general and under the afore-mentioned configurations, this paper studies the case of estimating the stiffness of fruit as an application domain. The study of different soft tissues is out of the scope of this paper.

3.1 Sensor tips configuration

Fig. 2(a) shows the configuration of the proposed tactile sensor in the plane. The proposed configuration is designed to have three cantilever beams, one of which corresponds to the *high stiffness spring* (with value K_h) and the other two correspond to the *low stiffness springs* (with value K_l). The former is located at the middle region between, and opposite end of, the latter; and all three beams are contiguous to each other. Moreover, each cantilever beam comprises a tip, at its end location, and a strain gauge, at the key source of its deflection. While each tip has the role of enabling the contact with the surface of the measured fruit specimen, each strain gauge has the role of converting the deflection of the corresponding beam into input voltages for signal conditioning.

Table 1. Inclination angles for kiwifruit specimens as in Fig. 3.

Profile segments	Inclination angle θ			
	Case 1	Case 2	Case 3	Case 4
Segment 1 (yellow)	4.56°	3.43°	4.56°	4.84°
Segment 2 (red)	4.47°	5.65°	4.55°	4.64°
Segment 3 (green)	2.99°	3.48°	1.15°	6.10 °

3.2 Inclination angle: surface roughness

In order to confirm the allowable inclination angle θ (depicted in Fig. 1(c)) of the kiwifruit specimens and to determine the Roughness Average (Ra) of the fruit's surface, a study of the surface roughness of kiwifruit using a 3D laser microscope [29] was conducted. It should be noted that the species of kiwifruit used throughout in this paper is the *Actinidia deliciosa*. The area of the fruit's surface examined under the microscope was $1000\ \mu m \times 1414\ \mu m$ with an average height of 340 µm, and a total of three samples were studied. Fig. 2(b) shows the 3D profiles of the scanned surfaces. By observing Fig. 2(b), the surface of kiwifruit is irregular with a plural number of peaks and valleys. The peaks are indicated by the red areas while the valleys are represented by the blue areas. Several sections were analyzed and the maximum Roughness Average (Ra) measured for kiwifruit was 29 µm, which is high compared to the typical surface roughness for smooth materials being usually below 5 µm [30]. Hence such high Ra is an indication that the surface of the fruit is far from being smooth. As a result of the irregularities of the kiwifruit surface, the inclination angle of the fruit was further studied in order to determine the maximum angle of contact between the sensor tips and the fruit surface.

Fig. 3 shows the peaks and valleys of the profiles studied. Straight lines were drawn across the surface of the fruit profiles with the laser microscope and the three sensor tips were simulated along the lines. The sensor tips are depicted by the three colour segments on the profile, that is yellow, red, and green. The colour segments are rendered by the microscope software across the measured profiles to show the inclination angles across the fruit's surface. Table 1 shows the corresponding inclination angles obtained from the 3D laser microscope software. The maximum inclination angle between the sensor tips and the kiwifruit surface was measured at different locations and found

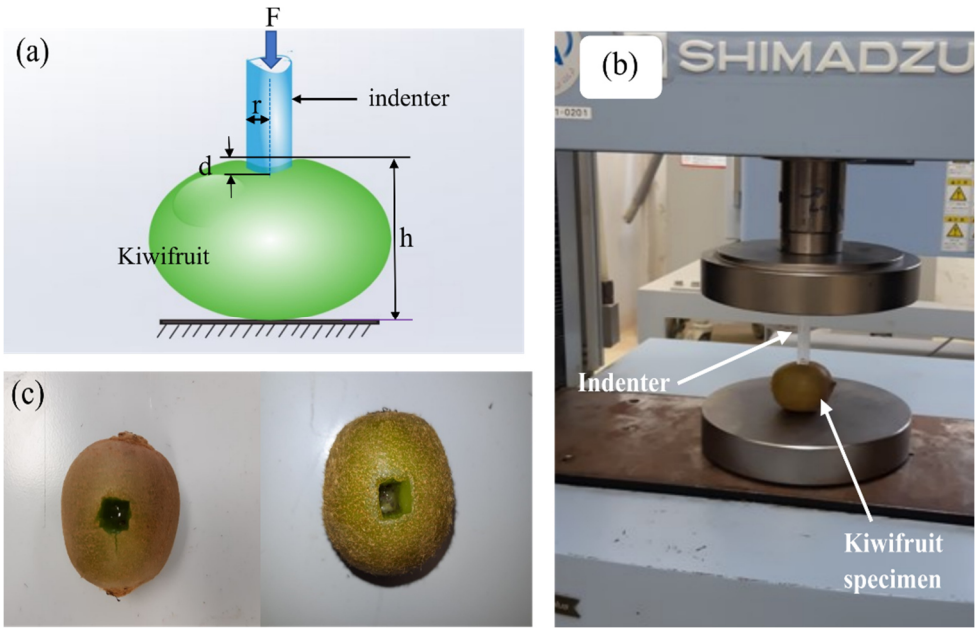

Fig. 4. (a) Schematic of kiwifruit with cylindrical indenter. (b) Loading of kiwifruit specimen on the UTM. (c) Kiwifruit after indentation.

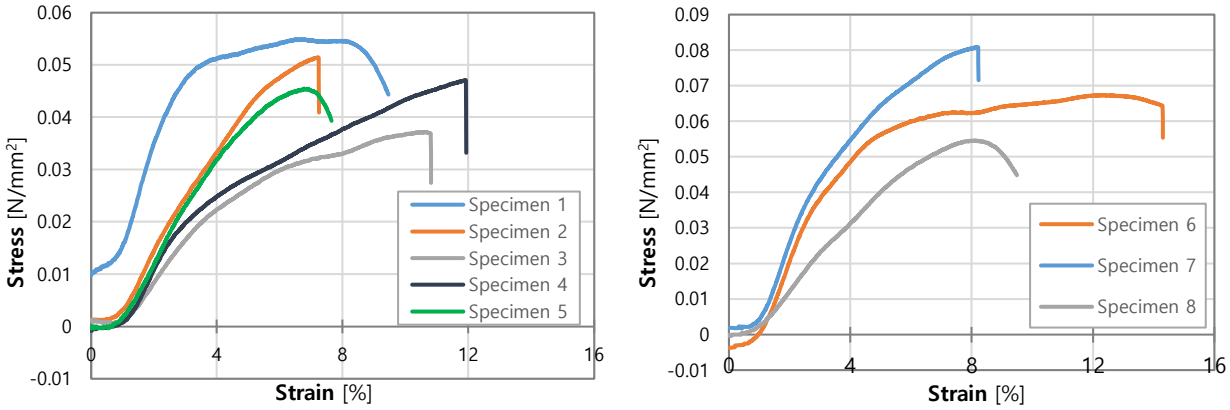

Fig. 5. Stress-strain curves of the compressed specimens.

to be around 6^0, as shown in Table 1. Although the large inclination angles are found to have an effect on the unstable output of cantilever-based stiffness sensors [31], the above-found upper bound of the inclination angle of the surface of specimens is relatively small for the application domain of this paper, since its tangent will render relatively small values in Eq. (5). And, along with a relatively small length L (as depicted in Fig. 1(c)), the term $L\tan\theta$ is expected to be of negligible value in Eq. (5).

3.3 Stiffness configuration: compression tests

A key notion behind the idea of estimating the stiffness of soft tissues is the realization of desirable stiffness for cantilever beam configuration. This section describes the considerations to set the allowable range for stiffness of kiwifruit specimens.

By performing compression tests on representative specimens of kiwifruit (*Actinidia deliciosa*) available, the allowable range of elastic modulus was estimated. Eight kiwifruit specimens were selected out of a large number based on a touch-based perception of maturity and softness of available kiwifruit. Their physical features (height and weight) are presented in Table 2. Although, studying a very large number of specimens over different seasons is relevant for practical contexts, this study rather focused on a smaller but yet representative set. The generalization to a large set of kiwifruit samples is straightforward.

The approach used in the compression test corresponds to the indentation-type, involving the indentation principle shown in Fig. 4(a) and whose setup is shown in Fig. 4(b). It should be noted that the species of kiwifruit used in this study has hairy skin, but the hair has no effect on the results of this study because the indentation principle is based on actual contact between the tissue of the specimen and the indenter or the sensor tips; the hairy skin of the fruit does not affect the contact conditions because the size of the hair is in the micro scale. Basically, the kiwifruit is subjected to a user-defined compression of force

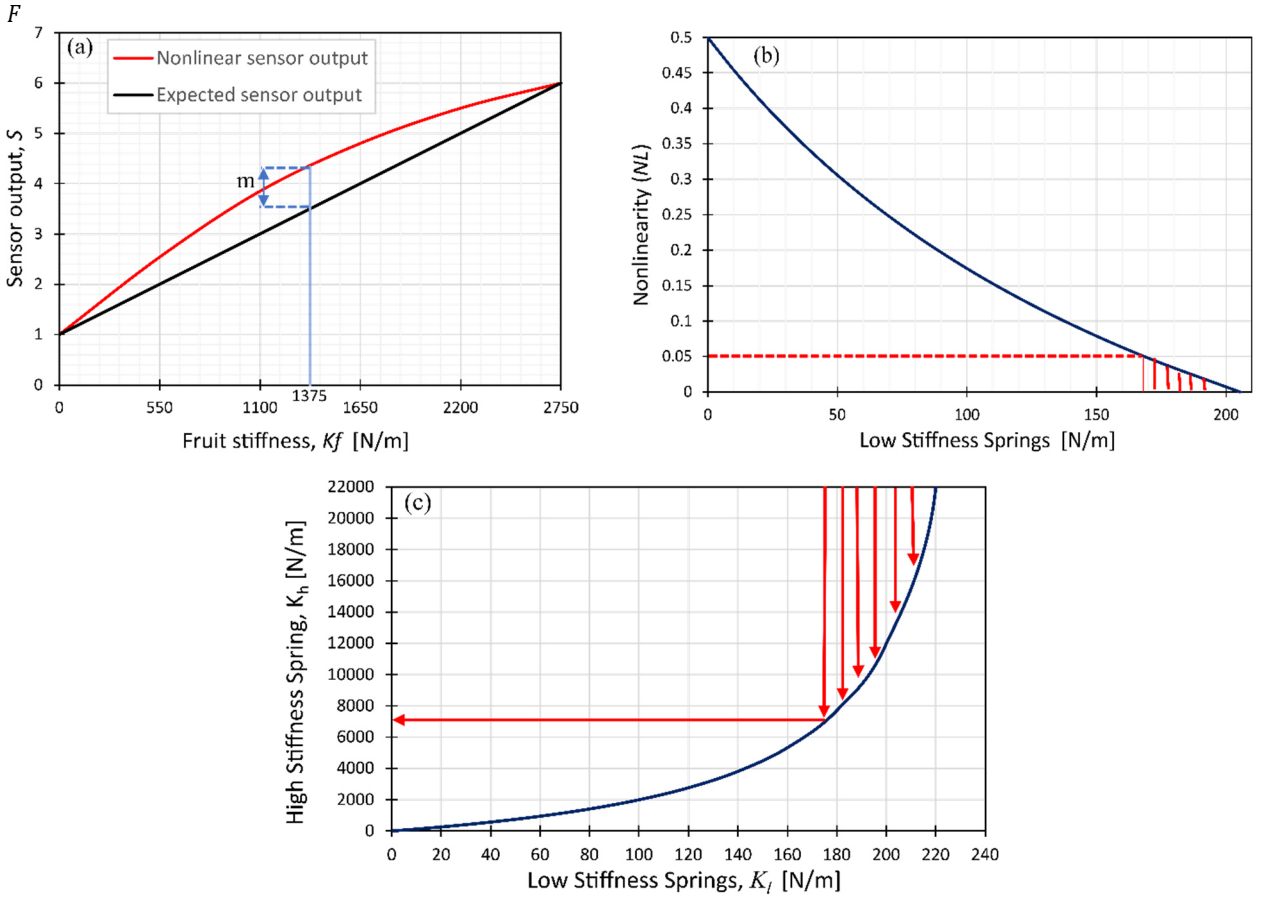

Fig. 6. (a) Nonlinear and expected sensor output vs. kiwifruit stiffness. (b) Nonlinearity vs. low stiffness springs, K_l. (c) High stiffness spring K_h vs. low stiffness springs K_l.

applied by an indenter of known geometry. Here, the fruit specimens were loaded radially on a Universal Testing Machine (UTM), Shimadzu model, and were compressed until failure. Fig. 4(c) shows two samples after compression tests, each of which shows the effect of the indentation process on the surface of the specimens. Then, the stress-strain profiles of the compressed specimens were obtained by considering the radial heights of the fruit and the surface area of the indenter. The modulus of elasticity for each compressed kiwifruit specimen was computed around the elastic region of the corresponding stress-strain curves, as shown in Fig. 5. The elastic modulus of a relevant set of kiwifruits, from the softest to the hardest, based on radial indentation, ranged from 0.88 MPa to 2.51 MPa as Table 2 shows. As such, Fig. 5 and Table 2 show that the stiffer (riper) the fruit is, the higher (lower) its elastic modulus is. It was also observed in the compression tests that the stiffer specimens experienced more force before failure than the softer ones, suggesting that their elastic moduli were directly related to their stiffness.

Table 2. Measured physical parameters, and the elastic modulus of a relevant set of kiwifruit (*Actinidia deliciosa*) specimens.

Specimen	Radial height [mm]	Radial width [mm]	Axial length [mm]	Weight [g]	Elastic modulus [MPa]
Specimen 1	46.68	55.5	58.17	68	2.07 ± 0.02
Specimen 2	49.00	52.57	57.00	65	1.21 ± 0.06
Specimen 3	46.40	52.42	52.57	60	0.88 ± 0.02
Specimen 4	43.83	54.67	55.89	65	1.22 ± 0.02
Specimen 5	40.50	43.50	54.00	63	1.17 ± 0.04
Specimen 6	52.00	51.00	63.85	70	2.33 ± 0.01
Specimen 7	48.00	51.50	66.00	72	2.51 ± 0.02
Specimen 8	47.70	57.13	63.50	62	1.13 ± 0.01

Furthermore, it is possible to estimate the stiffness of a soft body by using the elastic modulus derived from the indentation principle [32], as follows:

$$K_f = \frac{2r_i E_f C_k}{1-v^2} \tag{9}$$

where K_f denotes the stiffness of the specimen (kiwifruit), r_i denotes the indenter radius, E_f denotes the elastic modulus of the specimen, C_k denotes the value of the scaling factor, and v denotes the Poisson's ratio of the specimen. Then, by considering the following parameters: radius of the indenter $r_i = 0.5$ mm, elastic modulus $E_f = 2.51$ MPa, scaling factor $C_k = 1$, and Poisson ratio $v = 0.3$, the upper bound of the stiffness of the specimen becomes $K_f = 2750$ N/m (after substitution into Eq. (9)). Here,

- the specimen (kiwifruit) is assumed to be isotropic and linearly elastic, especially when the specimen is indented slightly with an indenter of small area,
- the Poisson's ratio was assumed to be $v = 0.3$ based on previous agricultural studies [33],
- the indenter was designed as a cuboid with side length of 1 mm, thus $r_i = 0.5$ mm,
- the scaling factor $C_k = 1$ is based on the indentation tests and finite element analysis reported by [34], and
- the elastic modulus $E_f = 2.51$ MPa is due to the upper bound of the compression test mentioned in Table 2.

3.4 Sensor output configuration

In line of the above, the key parameters in the sensor configuration become the stiffness K_h, K_l derived from Eq. (3) and Eq. (7), as well as the separating distance L between the sensing elements from Fig. 1(c), and the maximum output at the end of the measurement range S_{max}. The maximum output S_{max} can be computed by defining K_l and K_h at maximum K_f in Eq. (7); however, doing so increases the error in the sensor output S due to a crosstalk phenomenon, which causes a very large difference between K_l and K_h. A crosstalk analysis was studied by [27], where a maximum acceptable error of 10% was determined in the measurement process.

In order to portray the sensor output as a function of specimen stiffness, Fig. 6(a) shows the expected sensor output and the nonlinear output. Here, the relevant intervals are $K_f \in [0, 2750]$ N/m, $S \in [1, 6]$ and $L = 5$ mm due to the above-mentioned observations on the compression tests and the degree of feasible variation of sensor output. Fig. 6(a) is rendered based on the notion that a nonlinear behavior will occur despite the desirable and expected linear outcome. For practical scenarios, it is desirable that the relationship between S and K_f be linear, as shown by the dark line in Fig. 6(a) in order to maintain a constant sensitivity to stiffness along the measurement range. The maximum non-linearity error can be estimated as follows:

$$NL = \frac{m}{S_{max}-1} = \frac{(S_{1375}-1) - \left(\frac{S_{max}-1}{2}\right)}{S_{max}-1} \tag{10}$$

where NL denotes the nonlinearity error, S_{1375} represents the sensor output at the mid-range of the specimen stiffness considering $K_f \in [0, 2750]$ N/m, and m is the distance between the maximum point of nonlinearity to the corresponding point in the linear relationship.

In Fig. 6(a), when $S_{max} = 6$ and $K_f = 2750$ N/m, Eq. (10) becomes

$$NL = \frac{S_{1375} - 3.5}{5} \tag{11}$$

Also, from Eq. (7)

$$S_{1375} = \frac{K_h(K_l + 1375)}{2K_l(K_h + 1375)} \tag{12}$$

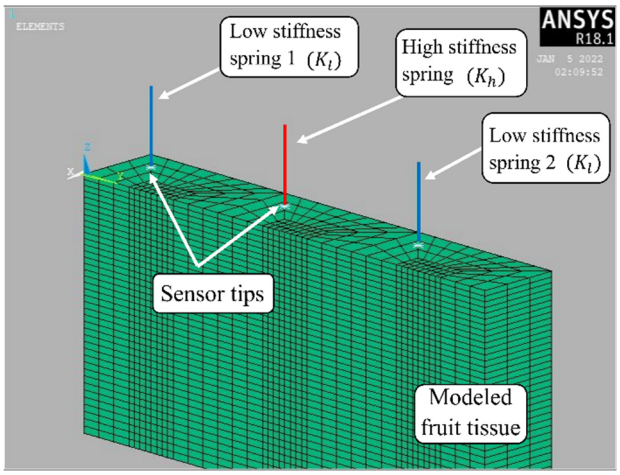

Fig. 7. Isometric view of the 3D axisymmetric finite element model.

And using Eq. (7), the relationship between K_l and K_h at S_{max} becomes

$$K_h = \frac{-2K_lK_fS_{max}}{K_l(2S_{max}-1) - K_f} \tag{13}$$

$$K_h = \frac{3000K_l}{250-K_l} \tag{14}$$

Now, substituting for K_h in Eq. (12) gives

$$S_{1375} = \frac{16500+12K_l}{2750+13K_l} \tag{15}$$

Finally, substituting for S_{1375} in Eq. (11) gives

$$NL = \frac{1375-6.7K_l}{2750+13K_l} \tag{16}$$

Eq. (16) relates the nonlinearity coefficient and the low stiffness spring of the sensor, whereas Eq. (14) relates the high stiffness spring and the low stiffness spring. To depict the nature of the above-mentioned relationships, Fig. 6(b) shows the plot of the nonlinearity NL as a function of the low stiffness spring, and Fig. 6(c) shows the plot of the *high stiffness spring* K_h as a function of the *low stiffness spring* K_l.

By observing at Figs. 6(b) and 6(c), one can notice that the *low stiffness spring* K_l is inversely (or directly) proportional to the nonlinearity NL (or the high stiffness spring K_h). As a consequence, from Fig. 6(c), high values of K_l are related to large values of K_h, implying that very low or insensitive values of the strain of the high stiffness sensor can be obtained, thus the very low or no output voltage. To avoid the insensitivity to strain values, an allowable nonlinearity coefficient of $NL = 5\%$ is acceptable [28]. Thus, substituting this coefficient into Eq. (16) yields $K_l = 175$ N/m. When this value is substituted into Eq. (14), it gives the corresponding value of $K_h = 7000$ N/m. Having selected the relevant values $K_l = 175$ N/m and $K_h = 7000$ N/m, a Finite Element Analysis (FEA) will be used to analyze the performance of the tactile sensor in the next section.

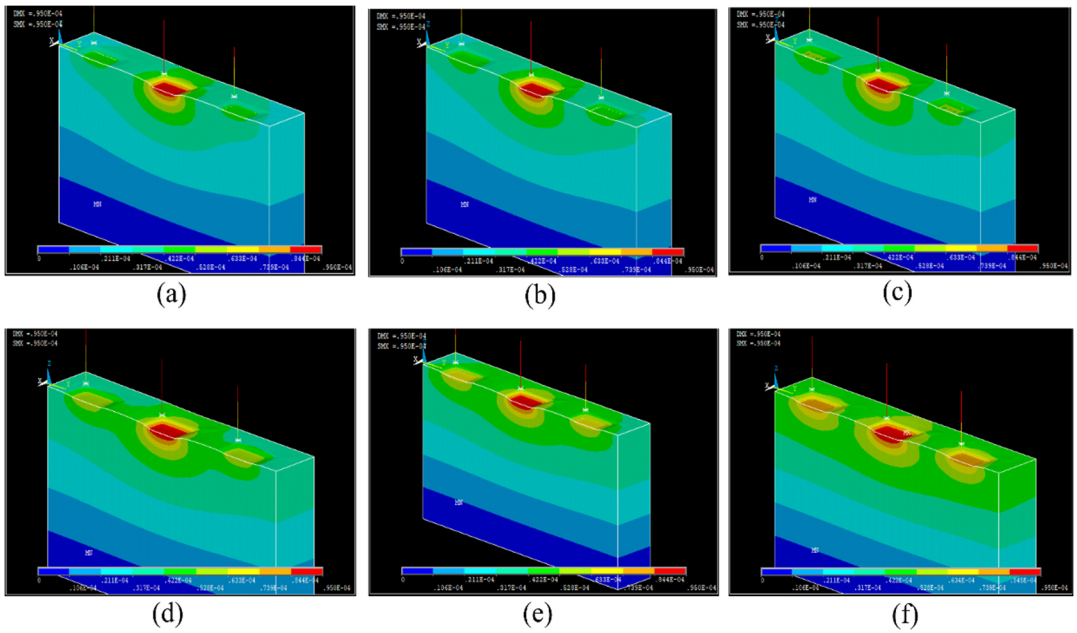

Fig. 8. Deformation of simulated fruit specimens of various elastic modulus E_f: (a) 3.0 MPa. (b) 2.5 MPa. (c) 2.0 MPa. (d) 1.5 MPa. (e) 1.0 MPa. (f) 0.5 MPa.

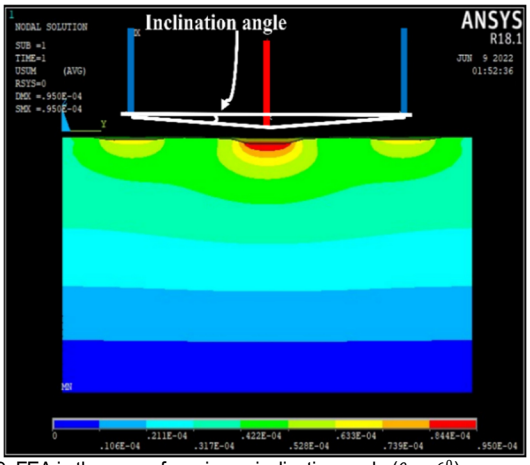

Fig. 9. FEA in the case of maximum inclination angle ($\theta = 6^0$).

3.5 Finite element modeling

In order to analyze the sensor performance in a dynamic simulation environment, it is relevant to use the stiffness parameters obtained in the previous section to implement a finite element model using the ANSYS Mechanical APDL (Ansys Parametric Design Language) software, as seen in Fig. 7. The fruit tissue was modeled and assumed to be homogeneous, isotropic and linearly elastic with Poisson's ratio of 0.3. For simplicity and without loss of generality, it was assumed that the fruit's body is fixed at its base. The model of the fruit was created using SOLID185 element, and a contact was established between the sensor tips and the fruit using the CONTA173 and TARGE170 elements located on the boundary of the fruit. Each of the three sensor tips were modeled using COMBIN14 elements which have the calculated stiffness of 175 N/m for each stiffness K_l component and 7000 N/m for the stiffness K_h (which correspond to the desired spring stiffness values described in section 3.4). Furthermore, meshing was done by applying the MESH200 element on the surface area of the fruit with contact zones highly reinforced.

For response analysis, six representative specimens of kiwifruit with elastic modulus E_f corresponding to 0.5 MPa, 1.0 MPa, 1.5 MPa, 2.0 MPa, 2.5 MPa, and 3 MPa were simulated. After the corresponding dynamic simulations with ANSYS software, Fig. 8 shows the slight deformation experienced by the fruit's tissues as a result of the contact between it and the sensor tips for all the various values of elastic modulus simulated. One can observe that the deformation on the simulated fruits increases as their modulus of elasticity decreases. The high stiffness sensor tips has more impact on the fruit compared to the low stiffness sensor tips as evidenced by the red regions on the modeled fruit surface. The 3.0 MPa kiwifruit which has a higher stiffness value is rigid enough to withstand deformation as evidenced in the small green regions on the modelled surface and around the sensor tips. On the other hand, the 0.5 MPa kiwifruit has a low stiffness value and experiences a higher deformation compared to fruits of higher elastic modulus. Albeit the deformation experienced by the fruit due to the sensor contact is very small (at 0.095 mm maximum) and has negligible effect on the fruit's mechanical properties; which implies that the sensor is good for non-destructive stiffness evaluation of other soft fruits. The results in Fig. 8 also confirm that the mechanical properties of fruits will decrease as their maturation increases. In addition, the sensor has been able to differentiate between all the various values of elastic modulus of kiwifruit that were simulated.

Fig. 10 shows the resulting sensor output S as a function of the applied displacement x for all the simulated kiwifruit at various elastic moduli. Two cases were considered: (1) without inclination angle, and (2) at 6^0 inclination angle as depicted

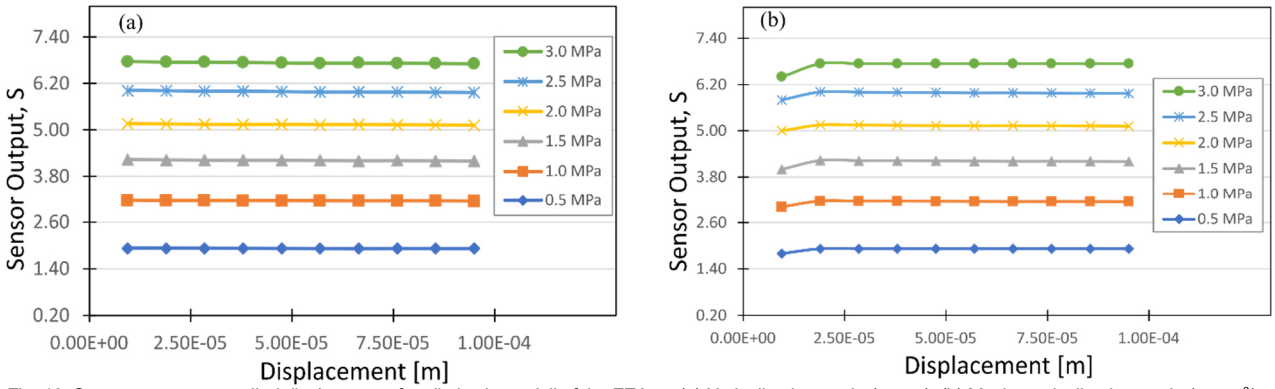

Fig. 10. Sensor output vs. applied displacement for all elastic moduli of the FEA at: (a) No inclination angle ($\theta = 0$); (b) Maximum inclination angle ($\theta = 6^0$).

Table 3. Sensor outputs and their corresponding stiffness values for the FEA.

Elastic modulus [MPa]	Sensor output S	Stiffness K_f [N/m]
0.5	1.92	549.78
1.0	3.14	1096.09
1.5	4.22	1650.19
2.0	5.14	2185.73
2.5	5.99	2743.04
3.0	6.74	3294.12

by Fig. 9. As shown in Fig. 9, the sensor tips were simulated to contact the modeled fruit tissue at different time, with the middle-high-stiffness spring contacting first. Because an irregular surface implies that the sensor tips will not contact the fruit's tissue at the same time. The high stiffness spring usually contacts first due to its central location and higher rigidity.

By observing Fig. 10(a), one will notice that the sensor output renders a relatively stable measurement value being independent of the applied displacement on the fruit for each elastic modulus. Also, in the case of maximum inclination angle (as in Fig. 10(b)), the output started off with a slightly lower value (due to the partial contact between the sensor tips and the fruit's tissue surface) but quickly stabilized in no time. The difference in both cases is negligible because there is no infinite or zero output along the displacement, and the sensor outputs are the same in both cases.

The above observations are a much-desired property in cantilever-based tactile sensing of soft tissues, and this will be explored further in subsequent sections. By using the corresponding constant values of the sensor output, the corresponding stiffness K_f of the modeled fruit tissue can be obtained based on Eq. (8). For the sake of clarity, Table 3 portrays the sensor output S and stiffness K_f for each case of the simulated elastic modulus.

3.6 Beam configuration

By using compliance-based studies, it is possible to determine the stiffness of each cantilever beam in Fig. 2(a), as follows:

$$K_b = \frac{E_b W_b t_b^3}{4L_b^3} \tag{17}$$

where

- b is a subscript representing either h, for the beam with *high stiffness*, or l, for the beam with *low stiffness*.
- K_b denotes the stiffness of the beam b,
- E_b denotes the elastic modulus of the material associated with beam b,
- L_b denotes the length of the beam b,
- W_b denotes the width of the beam b, and
- t_b denotes the thickness of the beam b.

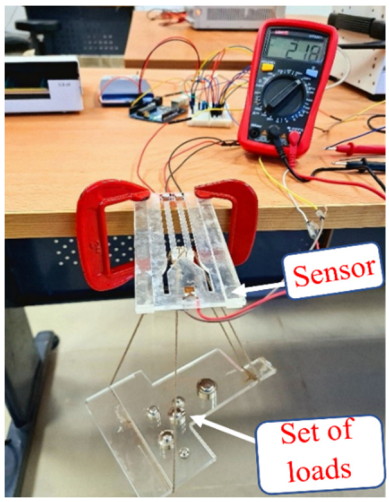

Fig. 11. Calibration setup.

The material constituting the prototype cantilever beams consists of acrylic Perspex, whose elastic modulus is $E_h = E_l = 3 \times 10^9$ N/m^2. The above implies that the elastic modulus in the *high stiffness spring* and the *low stiffness springs* are set to be equal. The motivation behind choosing acrylic Perspex is due to its ease of handling, biocompatibility, and the low cost to enable affordable prototype tactile sensor. By choosing the relevant thickness and dimensions of the cantilever beam, it is possible to realize user-defined stiffness being aligned with desirable *high stiffness spring* and the *low stiffness springs*. In order to achieve the desired spring stiffness $K_l = 175$ N/m and $K_h = 7000$ N/m (described in section 3.4), relevant dimensions were

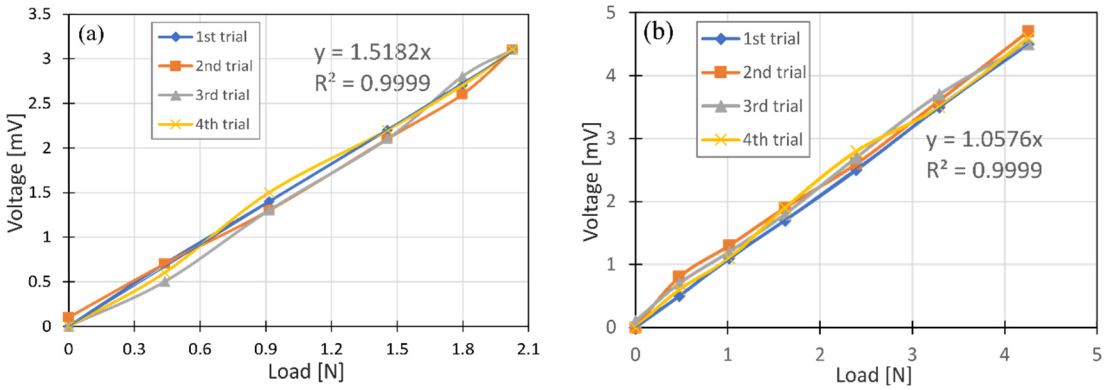

Fig. 12. Calibration curves for (a) the low stiffness sensor springs, and (b) the high stiffness sensor spring.

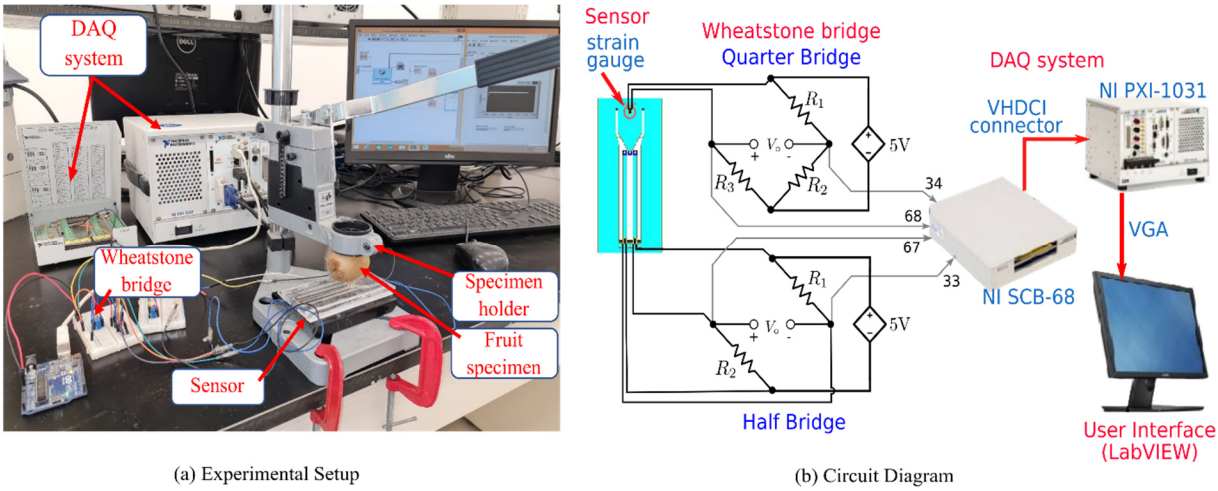

(a) Experimental Setup (b) Circuit Diagram

Fig. 13. Experimental setup, and system and circuit configuration of the sensor.

$t_h = t_l = 3$ mm, $L_l = 7.8$ cm, $L_h = 4$ cm, $W_l = 0.41$ cm, and $W_h = 2.2$ cm; where subscripts h and l denote the corresponding *high* and *low* stiffness values as in Eq. (17). The sensor tips, being cuboid in shape, have dimensions of 1 mm × 1 mm × 3 mm and are located at the free ends of the cantilever beams.

4. Experiments

In order to evaluate the feasibility to estimate the stiffness of soft tissue specimens by the designed sensor, a set of experiments were conducted which aims at measuring the stiffness of a variety of kiwifruit tissue. In this section, the experimental setup and insights obtained are presented.

4.1 Calibration

The high and low stiffness beams were calibrated separately by loading their free ends; the loads were suspended from the sensor tips using some strings as shown in Fig. 11. There were two Wheatstone bridges for the sensor – one quarter bridge for the high stiffness strain gauge, and a half bridge for the two low stiffness strain gauges. The quarter bridge comprised of three resistors with nominal resistance of 330 Ω each, while the half bridge had 2 resistors with nominal resistance of 330 Ω each. The strain gauge has a nominal resistance of 350 Ω and gauge factor of 2.02.

The high and low stiffness sensor springs were calibrated 4 times in order to ensure its stability, accuracy, and repeatability; Fig. 12 shows the calibration curves for the low and high stiffness sensor springs. The average voltage values of the repeated calibration were computed to give the calibration factor (as denoted by the equation on each of Figs. 12 (a) and (b)). These curves also show the load-voltage relationship of the sensor from which is obtained the calibration factor for the high and low stiffness sensor springs (with a coefficient of determination R^2 at 0.9999, which is acceptable for most practical scenarios). The calibration factor enables the proper conversion of measured output voltage of the sensor to the equivalent value of force. With the successful completion of the calibration procedure, the sensor was all set ready for experiments.

4.2 Setup and measurement

The experimental setup, as shown in Fig. 13(a), comprises a

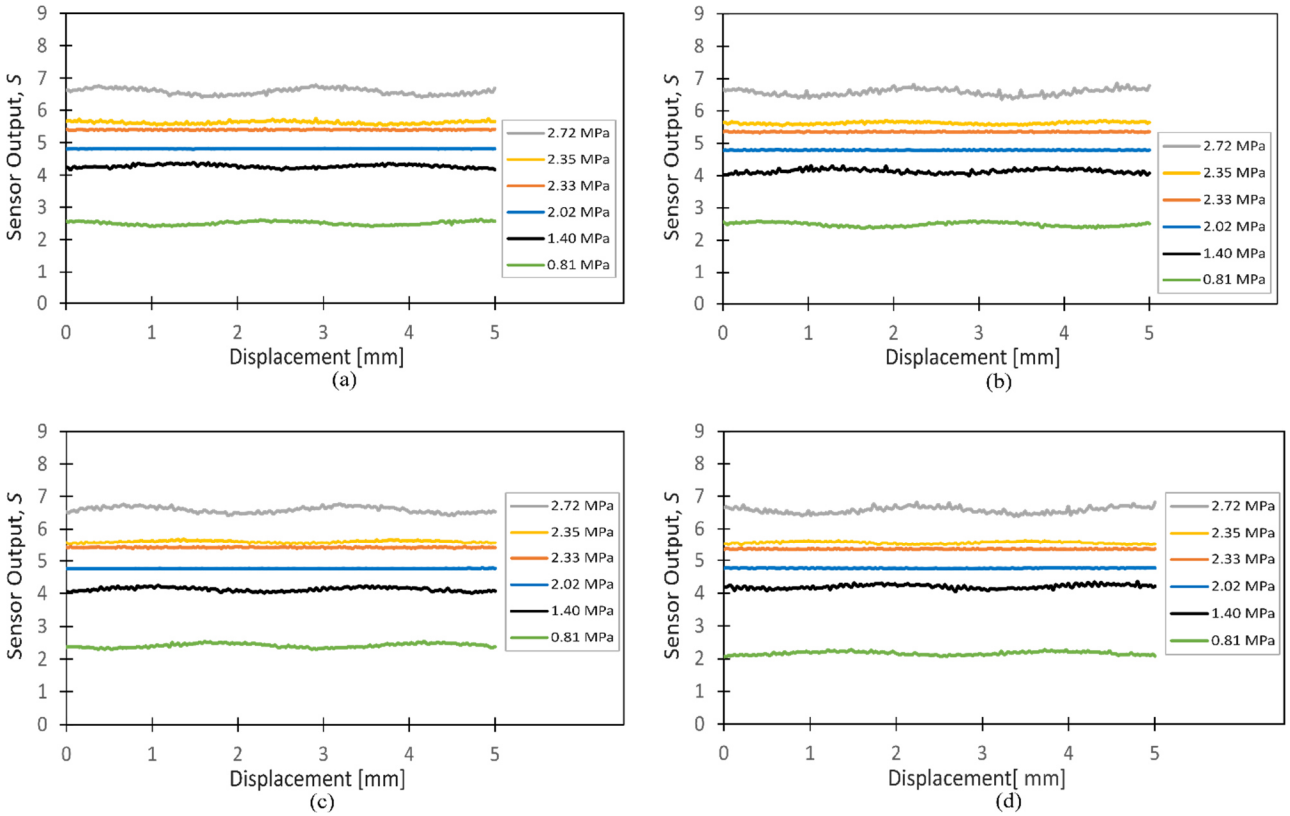

Fig. 14. Experimental sensor output for kiwifruit tissue of various elastic modulus E_f: (a) first trial (without inclination angle $\theta = 0$). (b) second trial (at maximum inclination angle $\theta_{max} \geq 6^{\circ}$). (c) third trial (at maximum inclination angle $\theta_{max} \geq 6^{\circ}$), and (d) fourth trial (without inclination angle $\theta = 0$).

data acquisition system (DAQ), Wheatstone bridge circuit, LCD screen (PC monitor), the sensor and specimen to be tested. The specimen holder has a displacement gauge which helps in measuring the applied displacement of the sensor on the fruit specimen. The sensor was fixed at its base using two C-clamps. When the fixed specimen was displaced vertically downward, it established contact with the fixed sensor and the displacement gauge shows the distance pushed from the point of contact. Once there is contact between the specimen and sensor, forces are generated which induce a strain in the sensor springs, thereby causing a change in resistance that is proportional to the induced strain. This resistance change is transmitted as output voltages through the Wheatstone bridge to the DAQ. The output voltages are converted to equivalent forces using the calibration factor of the high and low stiffness springs of the sensor in a block diagram programmed in the LabVIEW programme of the DAQ. The resulting forces are further converted into a readable output of the sensor using Eq. (7) which was programmed in the software and the output is displayed on the LCD screen. The circuit diagram of the sensor system is as shown in Fig. 13(b).

For simplicity and without loss of generality, six kiwifruit specimens at different ripeness levels and known elastic moduli were used. Basically, each specimen was pushed against the sensor tips at a maximum displacement of 5 mm from its point of contact with the sensor. The stiffness of each fruit specimen was evaluated repeatedly by four consecutive and independent tests (denoted as trials) at different points on the specimen's surface in order to ensure repeatability and robustness of the sensor. In order to show the sensor's ability to tackle the inclination angle without loss of performance, the stiffness measurement was repeated twice at points of maximum inclination angle $\theta_{max} \geq 6^{\circ}$. The elastic modulus E_f of the six kiwifruit specimens were 2.72 MPa, 2.35 MPa, 2.33 MPa, 2.02 MPa, 1.40 MPa, and 0.81 MPa, respectively, each of which were obtained through a compression test by a Universal Testing Machine (UTM). The key motivations of performing compression tests on the specimens was so as to compare the elastic modulus obtained from the UTM to that of the corresponding stiffness derived from the output of the sensor.

5. Final results and discussion

The experiments evaluated the feasibility of the proposed sensor configuration to estimate the stiffness of a relevant set of soft body (fruit tissue) specimens by conducting four independent measurements with the sensor (four trials) and the results are as shown in Fig. 14. Each of Figs. 14(a) – (d) shows the measured sensor output S as a function of induced displacement x on the fruit specimens. It should be noted that, for cantilever-based stiffness sensors, it is desired to have a horizontal line when the sensor output is plotted against displacement (as

a sign of stability). While Figs. 14(a) and (d) show the outputs of the sensor when the measurement was done at points of zero inclination angle of the fruit surface, Figs. 14(b) and (c) show the sensor outputs at points of maximum inclination angle (i.e., at $\theta_{max} \geq 6^{\circ}$). From these figures, the following observations can be noted:

i. the sensor output S remained stable throughout the displacement and is independent of both the inclination angle and applied displacement of the sensor on the soft body (fruit) as evidenced by the horizontal lines of the curves,
ii. the sensor output remained stable for arbitrary number of independent trials, and
iii. negligible fluctuations were recorded in some of the cases (at 2.72 MPa and 0.81 MPa), since they were caused by inherent measurement noise during the signal acquisition.

Compared to previous studies in [23], [26], [27], [28], the outputs of the sensor proposed in this paper (when tested experimentally) show a reasonable level of stability and repeatability over independent trials. The results in Fig. 14 clearly show that softer kiwifruit of elastic modulus less than 1 MPa (which are the ripest and softest in the market) have an output ranging between 2 and 3. On the other hand, fresh kiwifruit which have elastic modulus of over 2.5 MPa (harder kiwifruit) give an output range between 6 and 7. Using Eq. (8), the corresponding stiffness values of the fruit are computed as shown in Table 4. By looking at Table 4, it can be seen that the fruit tissue stiffness increases with higher sensor output, which is in line with the theoretical observations based on the FEA in section 3.5. On the other hand, Table 4 also shows the error percentage between the analytical sensor output S_A (i.e., based on the known modulus of elasticity of the fruit) and the experimental sensor output S. By looking at the error rates in Table 4, it can be observed that the error ranged from 0.18% to 3.50%, which is reasonable compared to the work of previous research attaining the error rate of up to 14% [28]. Meanwhile, Table 4 and Fig. 15 depict the accuracy of the sensor's performance, with minimum and maximum values being 96.50% and 99.81% respectively, which is also reasonable and competitive. The maximum accuracy was observed for kiwifruit of stiffness 2538.78 N/m while the minimum accuracy was observed for kiwifruit of stiffness 2355.72 N/m.

Table 4. Measured kiwifruit stiffness properties, their accuracy and error rates between analytical and experimental sensor outputs.

Elastic modulus, E_f [MPa]	Stiffness of kiwifruit, K_f [N/m]	Experimental output, S	Analytical output, S_A	Error [%]	Accuracy [%]
2.72	3066.37	6.44	6.33	1.74	98.28
2.35	2538.78	5.69	5.70	0.18	99.81
2.33	2355.72	5.50	5.70	3.50	96.50
2.02	2063.75	4.94	5.10	3.13	96.89
1.40	1590.31	4.11	4.01	2.49	97.53
0.81	836	2.61	2.70	3.33	96.67

The above-mentioned results show that the proposed sensor configuration not only offers a more stable output for distinct displacement x over independent trials, but also offers small error rates in soft tissue stiffness measurement. The approach here is based on, and supported by observations on the inclination angle, compression tests, mathematical modeling, FEM, and compliance-related detection.

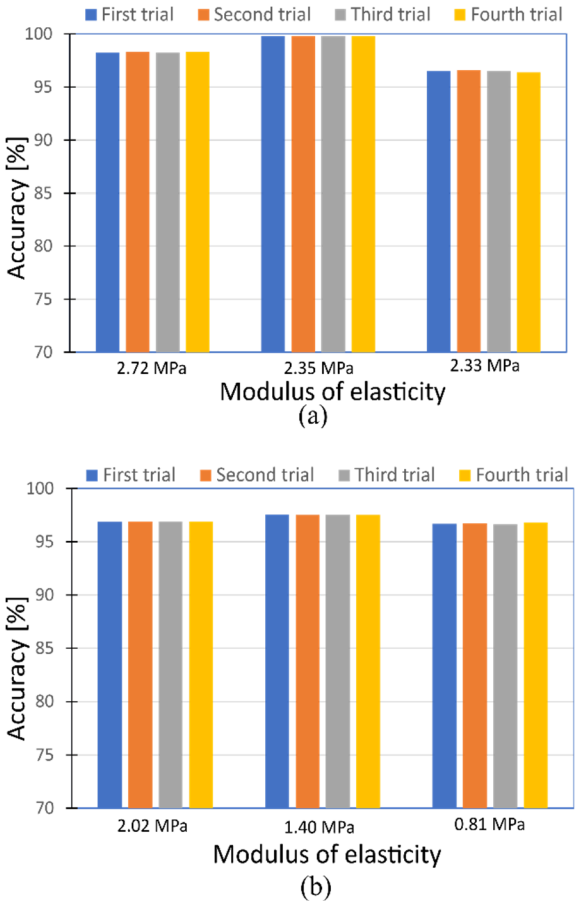

Fig. 15. Accuracy of the experimental sensor outputs for (a) 2.72 MPa, 2.35 MPa, and 2.33 MPa, (b) 2.02 MPa, 1.40 MPa, and 0.81 MPa.

5.1 Future outlook

The approach presented in this study has demonstrated the possibility of achieving stable sensor readings that are independent of the inclination angle and irregularity of soft tissue surfaces. Although the kiwifruit was used as a case study, the results show that the proposed sensor configuration is potential for the design of general and tailored stiffness sensors for fruit sorting, quality control, and ripeness measurement applications. The approach could also be useful in a wider range of soft tissue stiffness measurement applications; for example, in robotic sensing, and medical diagnosis applications (such as minimally-invasive surgeries).

In the future work, the design concept will be expanded to study the sensor's performance with different kinds of soft tissues. Also, tailored signal processing techniques aiming at finding the nonlinear relations between the obtained sensor output and the elastic modulus will be studied, which is potential in deriving closed form expressions for stiffness of soft tissues in general, and for understanding the sensor's sensitivity, reliability, and measurement range in many applications.

6. Conclusions

This paper has proposed a tactile sensor configuration for estimating the stiffness of soft tissues under maximum values of inclination angle of their surface (at $\theta_{max} \geq 6^{\circ}$). In particular, this paper has demonstrated the feasibility of the proposed configuration for the measurement of soft tissue stiffness using kiwifruit as a case study. By using observations from the inclination angle, mathematical analyses, Finite Element modeling, and compliance-based principles, the study devised a suitable configuration for a cantilever spring-based tactile sensor that achieves stable measurement at distinct displacements over independent trials. The results of the Finite Element analysis and experimental validation show that the sensor achieves relatively stable outputs that are independent of the inclination angle of the fruit's tissue. This pinpoints the novelty of the proposed sensor and its configuration. Furthermore, the sensor also achieves minimum error with respect to the analytical observations, and a maximum accuracy of 99.81%. Therefore, the performance of the proposed sensor, in stiffness measurement, portray superiority when compared with the most recent state-of-the-art similar studies mentioned earlier.

The results, in terms of variability of sensor readings under diverse sensing conditions, show that the sensor configuration and design approach are relevant in the design of new stiffness sensor architectures that are specifically tailored to soft tissue stiffness measurement. The potential applications of this specific study are in the areas of robotics (artificial robotic skin), minimally-invasive surgery, agricultural robots for real-time fruit sorting and quality control, amongst others. The future work will focus on studying the performance of the sensor on different kinds of soft tissues, as well as mechanisms to find the nonlinear relations between the obtained sensor output and the elastic modulus, both of which are potential to understanding the sensor's sensitivity, reliability, and measurement range in many applications.

Acknowledgments

This study was supported, for the first author, by the Egypt-Japan University of Science and Technology (E-JUST) scholarship, co-sponsored between the Egyptian Ministry of Higher Education (MoHE) and the Japan International Cooperation Agency (JICA). The authors thank the Science and Technology Development Fund (STDF-12417 project) of the Egyptian Ministry of Scientific Research for providing the equipment used in this research at the Micro Fabrication Centre of E-JUST.

Nomenclature

θ	: Inclination angle between sensor and the fruit tissue
θ_{max}	: Maximum inclination angle
$\tilde{\theta}$	: Vertical component angle due to the inclination
C_k	: Scaling factor
E_f	: Elastic modulus of the fruit
F_H	: High stiffness spring force
F_L	: Low stiffness spring force
K_f	: Fruit tissue stiffness
K_h	: High stiffness spring constant
K_H	: Equivalent high stiffness spring
K_l	: Low stiffness spring constant
K_L	: Equivalent low stiffness spring
L	: Distance between the sensor tips
NL	: Nonlinearity error
Ra	: Roughness average of the fruit's tissue surface
r_i	: Indenter radius
S	: Sensor output
S_{max}	: Maximum output at end of measurement range
v	: Poisson's ratio
x	: Applied displacement of the sensor

References

[1] L. Kitinoja, S. Saran, K. Roy and A. A. Kader. Postharvest technology for developing countries: challenges and opportunities in research, outreach and advocacy. *Journal of the Science of Food and Agriculture,* 91 (4) (2011) 597-603.

[2] Y. Chen, W. L. Cai, X. J. Zou and H. P. Xiang, Extrusion mechanical properties of fresh litchi, *Transactions of the Chinese Society of Agricultural Engineering*, 27 (8) (2011) 360–364.

[3] S. Tian, J. Wang and H. Xu, Firmness measurement of kiwifruit using a self-designed device based on acoustic vibration technology, *Postharvest Biology and Technology*, 187 (2022).

[4] A. H. Gómez, G. Hu, J. Wang and A. G. Pereira, Evaluation of tomato maturity by electronic nose, *Computers and Electronics in Agriculture*, 54 (1) (2006) 44–52.

[5] E. H. Yossy, J. Pranata, T. Wijaya, H. Hermawan and W. Budiharto, Mango fruit sortation system using neural network and computer vision, *Procedia Computer Science*, 116 (2017) 596-603.

[6] M. Shiddiq, F. Fitmawati, R. Anjasmara, N. Sari and Hefniati, Ripeness detection simulation of oil palm fruit bunches using laser-based imaging system, *The 6th International Conference on Theoretical and Applied Physics (The 6th ICTAP)* (2017).

[7] M. Dadwa and V. K. Banga, Color image segmentation for fruit, *2nd International Conference on Electrical, Electronics and Civil Engineering*, Singapore (2012).

[8] Q. Meng, J. Shang, R. Huang, and Y. Zhang, Determination of soluble solids content and firmness in plum using hyperspectral imaging and chemometric algorithms, *Journal of Food Process Engineering*, 44 (1) (2021). DOI: 10.1111/jfpe.13597

[9] Y. Dong, Y. Huang, B. Xu, B. Li, and B. Guo, Bruise detection and classification in jujube using thermal imaging and densenet, *Journal of Food Process Engineering*, (2021). DOI: 10.1111/jfpe.13981

[10] H. Kang and C. Chen, Fast implementation of real-time fruit detection in apple orchards using deep learning, *Computers and Electronics in Agriculture*, 168 (2020). https://doi.org/10.1016/j.compag.2019.105108

[11] F. J. García-Ramos, C. Valero, I. Homer, J. Ortiz-Cañavate and M. Ruiz-Altisent, Non-destructive fruit firmness sensors: a review, *Spanish Journal of Agricultural Research,* 3 (1) (2005) 61-73.

[12] F. Zahed, A. Mohammad and H. B. S. Reza, Nondestructive methods for determining the firmness of apple fruit flesh, *Information Processing in Agriculture,* 8 (4) (2021) 515-527.

[13] J. Sun, R. Künnemeyer and A. McGlone, Optical methods for firmness assessment of fresh produce: a review, *Postharvest Handling,* IntechOpen, London, UK, (2017).

[14] T. Shijie and X. Huirong, Mechanical-based and Optical-based methods for nondestructive evaluation of fruit firmness, *Food Reviews International,* (2022).

[15] A. Fekete and J. Felf˙oldi, Firmness-based expert system for fruit quality assessment, *IFAC Proc. Volumes* (1998), 61-65.

[16] H. Zhu, L. Yang, J. Fei, L. Zhao L and Z. Han, Recognition of carrot appearance quality based on deep feature and support vector machine, *Computers and Electronics in Agriculture,* 186 (2021).

[17] H. Zhu, L. Yang, Y. Sun and Z. Han, Identifying carrot appearance quality by an improved dense capnet, *Journal of Food Process Engineering,* 44 (1) (2021).

[18] T. Kunpeng, S. Cheng, L. Xianwang, H. Jicheng, C. Qiaomin and Z. Bin, Mechanical properties and compression damage simulation by finite element for kiwifruit, *International Agricultural Engineering Journal*, 26 (4) (2017) 193-203.

[19] A. Jahanbakhshi, R. Yeganeh and G. Shahgoli, Determination of mechanical properties of banana fruit under quasi-static loading in pressure, bending, and shearing tests, *International Journal of Fruit Science,* 20 (3) (2020) 314-322.

[20] G. Shahgholi, M. Latifi and A. Jahanbakhshi, Potato creep analysis during storage using experimental measurement and finite element method (fem), *Journal of Food Process Engineering,* 43 (2020).

[21] C. T. Nnodim, A. M. R. Fath ElBab, B. W. Ikua and D. N. Sila, Design, simulation, and experimental testing of a tactile sensor for fruit ripeness detection, *Transactions on Engineering Technologies*, Springer Nature Singapore, (2021) 59-73.

[22] C. T. Nnodim, A. M. R. Fath El-Bab, B. W. Ikua and D. N. Sila, Estimation of the modulus of elasticity of mango for fruit sorting, *International Journal of Mechanical & Mechatronics Engineering*, 19 (2) (2019) 1-10.

[23] C. T. Christopher, A. M. R. FathElbab, C. O. Osueke, B. W. Ikua, D. N. Sila and A. Fouly, A piezoresistive dual-tip stiffness tactile sensor for mango ripeness assessment, *Cogent Engineering,* 9 (1) (2022).

[24] T. Tsuji, Y. Kaneko and S. Abe, Whole-body force sensation by force sensor with shell-shaped end-effector, *IEEE Transactions on Industrial Electronics,* 56 (5) (2009) 1375-1382.

[25] A. Esmaeel, K. I. E. Ahmed and A. M. R. FathEl-Bab, Determination of damping coefficient of soft tissues using piezoelectric transducer, *Biomedical Microdevices*, 23 (2) (2021).

[26] A. M. Fath El-Bab, M. E. Eltaib, M. M. Sallam and O. Tabata, Tactile sensor for compliance detection, *Sensors and Materials*, 19 (3) (2007) 165-177.

[27] A. Fath El-Bab, T. Tamura, K. Sugano, T. Tsuchiya, O. Tabata, M. E. H. Eltaib and M. Sallam, Design and simulation of a tactile sensor for soft-tissue compliance detection, *IEEJ Transactions on Sensors and Micromachines*, 128 (5) (2008) 186-192.

[28] A. Fouly, A. Fath El-Bab, M. Nasr, and A. Abouelsoud, Modeling and experimental testing of three-tip configuration tactile sensor for compensating the error due to soft tissue surface irregularities during stiffness detection, *Measurement*, 98 (2017) 112-122.

[29] The American Society of Mechanical Engineers (ASME), *Surface Texture (Surface Roughness, Waviness, and Lay)*, ASME, New York, (2020).

[30] S. Hall, 1-fluid flow, *Branan's Rules of Thumb for Chemical Engineers*, 5th Ed., Butterworth-Heinemann, Oxford, (2012) 1-26 https://doi.org/10.1016/B978-0-12-387785-7.00001-3

[31] A. Fouly, A. M. R. Fath El Bab, A. A. Abouelsoud and M. N. Nasr, Error source identification in measuring soft tissue stiffness and self compensating this error using three probes configuration, *7th IEEE International Conference on Intelligent Systems, Modelling and Simulation*, (2016).

[32] W. C. Hayes, L. M. Keer, G. Herrmann, and L. F. Mockros, A mathematical analysis for indentation tests of articular cartilage, *Journal of Biomechanics*, 5 (5) (1972) 541-551.

[33] Z. E. Zhou, *Physical Properties of Agricultural Materials*, China Agricultural Press, Beijing (1994).

[34] M. Zhang, Y. P. Zheng and A. F. T. Mak, Estimating the effective young's modulus of soft tissues from indentation tests - nonlinear finite element analysis of effects of friction and large deformation, *Medical Engineering and Physics*, 19 (6) (1997) 512-517.

Author information

Frank Efe Erukainure is a postgraduate Research Student at the Department of Mechatronics and Robotics Engineering, Egypt-Japan University of Science and Technology, Alexandria, Egypt. Also, he is currently a Graduate Assistant lecturer at Federal University Otuoke, Bayelsa State, Nigeria. His research interests include MEMS/NEMS, Machine Learning, Mechatronics & Robotic systems design, and Artificial Intelligence.

Victor Parque is an Associate Professor at the Department of Modern Mechanical Engineering, Waseda University, as well as a JSUC Visiting Professor at Egypt-Japan University of Science and Technology. He obtained the Ph.D. from the Graduate School of Information, Production and Systems, Waseda University, 2011. He was a Post-Doctoral Fellow at the Department of Mechanical Engineering, Toyota Technological Institute in 2012-2014. His research interests span the principles of Learning Systems and Artificial Intelligence and its applications to Design Engineering, Planning and Control.

Mohsen A. Hassan is a Professor at the Department of Materials Science and Engineering, Egypt-Japan University of Science and Technology, Egypt. He received the master's degree in 1998 (Egypt), and the PhD in Information and Production Science (forming technology) at Kyoto Institute of Technology, Japan. He has published more than 180 research articles in the field of material models, modelling and simulation, forming and micro forming, MEMS, Piezoelectric thin Films, heart mechanics, ceramics processing and rubbers.

Ahmed M. R. FathEl-Bab is a Professor at the Department of Mechatronics and Robotics Engineering, Egypt-Japan University of Science and Technology, Alexandria, Egypt. He received the M.Sc. and Ph.D. degrees from Assiut University, Egypt, in 2002 and 2008 respectively. From October 2006 – October 2008, he was a Visiting Researcher at the Tabata Laboratory, Kyoto University, Japan. During this period, he gained practical experience in the microfabrication of MEMS/NEMS. His current interests include microsensors (principles, simulation, design, and fabrication), micromachining and its application in MEMS, tactile sensing systems (tactile sensing and display), micro energy harvesting devices, and Micro fluidic systems.